



A multi-spectroscopic and molecular docking approach for DNA/protein binding study and cell viability assay of first-time reported pendent azide bearing Cu(II)-quercetin and dicyanamide bearing Zn(II)-quercetin complexes

Anupam Mudi^a, Shubham Ray^b, Manjushree Bera^c, Malay Dolai^b, Manik Das^b, Pronab Kundu^d, Soumik Laha^e, Indranil Choudhuri^f, Bidhan Chandra Samanta^g, Nandan Bhattacharyya^f, Tithi Maity^{b,*}

^a Department of Botany, Behala College, Behala, India

^b Department of Chemistry, Prabhat Kumar College, Contai, Contai, Purba Medinipur, 721404, India

^c Department of Nutrition, Prabhat Kumar College, Contai, Contai, Purba Medinipur, 721404, India

^d Department of Chemistry, Presidency University, Yelahanka, Bengaluru, 560064, India

^e IICB, Kolkata, West Bengal, India

^f Panskura Banamali College, Panskura, West Bengal, India

^g Department of Chemistry, Mugberia Gangadhar Mahavidyalaya, Purba Medinipur, India

ARTICLE INFO

Keywords:

Quercetin
Metal complex
DNA/protein binding
Cell viability

ABSTRACT

In the current study, one new quercetin-based Zn(II) complex [Zn(Qr)(CNNCN)(H₂O)₂] (Complex 1) which is developed by condensation of quercetin with ZnCl₂ in the presence of NaN(CN)₂ and Cu(II) complex [Cu(Qr)N₃(CH₃OH)(H₂O)] (complex 2) which is developed by the condensation reaction of quercetin and CuCl₂ in presence of NaN₃, are thoroughly examined in relation to their use in biomedicine. The results of several spectroscopic studied confirm the structure of both the complexes and the Density Functional Theory (DFT) study helps to optimize the structure of complex 1 and 2. After completion of the identification process, DNA and Human Serum Albumin (HSA) binding efficacy of both the investigated complexes are performed by implementing a long range of biophysical studies and a thorough analysis of the results unveils that complex 1 has better interaction efficacy with the macromolecules than complex 2. The binding efficacy of complex 1 is comparatively higher towards both macromolecules because of its pure groove binding mode during interaction with DNA and the presence of an extra H-bond during connection with HSA. The experimental host-guest binding results is fully validated by molecular docking study. Interestingly complex 1 shows better antioxidant properties than complex 2, as well as quercetin, and it has strong anticancer property with minimal damage to normal cells, which is proved by the MTT assay study. Better DNA and HSA binding efficacy of 1 may be the reason for the better anticancer property of complex 1.

* Corresponding author.

E-mail address: titlipkc2008@gmail.com (T. Maity).

<https://doi.org/10.1016/j.heliyon.2023.e22712>

Received 27 September 2023; Received in revised form 16 November 2023; Accepted 16 November 2023

Available online 28 November 2023

2405-8440/© 2023 Published by Elsevier Ltd.

This is an open access article under the CC BY-NC-ND license

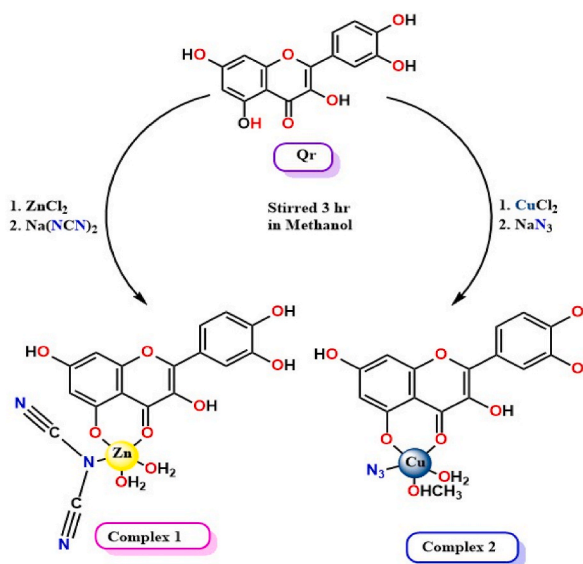
(<http://creativecommons.org/licenses/by-nc-nd/4.0/>).

1. Introduction

In drug development research DNA is the primary target of the drug molecule as after association with DNA the drug molecule can hinder the quick replication of the DNA [1–4]. Simultaneously high toxicity to normal cells after consuming the drug is a matter of concern to the scientific community and the reduction of the side effect of the drug molecule is a challenging issue to the researchers [5, 6]. Using a drug delivery system is the most acceptable pathway to reduce the side effects because the vehicle can transport the molecule to the target place without giving any scope of release the molecule to the normal. The prevalent protein in the blood is HSA and it is recognized as a drug transporter [7–10]. Thus, prior to reviewing the biological application, verifying the compounds' ability to bind DNA and HSA is crucial in order to assess their suitability for application in therapeutics. Flavonoids are a diverse class of polyphenolic compounds that are frequently found in nature and have fascinating physicochemical properties. These compounds are beneficial to human health because of their biological properties, which include activity against HIV, influenza, and bacteria [11–15]. Generally, flavonoids comprises two aromatic rings and a heterocycle that contains oxygen. The presence of several bioactivities in terms of anti-oxidant, anti-cancer, anti-inflammatory, anti-diabetic, anti-atherosclerotic, and anti-apoptotic capabilities, flavonoids attract the scientific community to carry out interface research in chemistry and biology [16–18]. Flavonoids are recognized anticancer material and it is already proved that these compounds create obstacles to some particular stages of the carcinogenic process with the reduction of cell growth [19–23]. Quercetin (3,3',4',5,7 pentahydroxyflavone) is one of numerous physiologically significant flavonoids that has been the subject of much investigation and notable sources of this well-known flavonoid include apples, red grapes, onions, raspberries, honey, cherries, citrus fruits, and green leafy vegetables. It's interesting to note that it is a well-known anticancer agent and that its mechanism of cell death is also disclosed [24,25]. The use of cisplatin as an effective anticancer drug, inspires the scientific community to develop several metal-based compounds with effective biological applications [26–32]. At the same time, many quercetin-metal complexes are synthesized and inspected with respect to their DNA and HSA binding efficacy [33–36]. But no literature report is obtained where the quercetin-metal complex with one ancillary ligand has been developed, although it is well established that the presence of ancillary ligands like azide, thiocyanate, and dicyanamide in the metal center enhances the DNA/HSA binding efficacy [37–40]. Therefore, it is reasonable to anticipate that the addition of an ancillary ligand will improve the ability of quercetin metal complexes to bind with macromolecules (see Scheme 1).

At the same time, the several side effects of cisplatin [41] boost chemists to develop nonplatinum metal complexes with effective biomedical applications. It is already proved that in anticancer drug development research, Cu and Zn complexes are acceptable non-platinum metal complexes [42–47] with effective anticancer properties. A thorough search discloses that Cu-quercetin and Zn-quercetin complexes have been already studied with respect to their DNA and HSA binding. But not no study has been done where metal quercetin complexes with ancillary ligands are developed and inspected for their efficacy checking towards DNA/HSA binding and anticancer properties on both cancer cells and normal.

Considering all the points, discussed above, herein the synthesis, identification, and bio medical application of one pendant dicyanamide bearing Zn(II) (complex 1) and azide bearing Cu(II) (complex 2) are demonstrated. DFT analysis optimizes the structures of both the complexes and the oxidation state of complex 2 has been confirmed by the EPR study. Following structural confirmation, techniques such as UV, fluorescence, and CD titration are used to measure the DNA/HSA binding efficiency of the complexes under study. The results of all the biophysical studies approve the fact that both complexes can effectively bind with both macromolecules. But the association ability of complex 1 is comparatively better than 2. Additionally, complex 1 has a good antioxidant properties than



Scheme 1. Synthesis of complex 1 and 2.

complex 2 and quercetin. Finally, the cell viability of both complexes has been done by implementing an MTT assay study on HeLa cells and normal HEK cells and the results show that complex 1 has effective anticancer properties with low toxicity to the normal cell.

2. Results and discussions

2.1. Synthesis, IR, UV and ESI-MS analyses of the complexes

Complex 1 has been developed by the reaction of quercetin and ZnCl_2 in the presence of sodium dicyanamide whereas complex 2 is developed by the reaction of quercetin and CuCl_2 in the presence of sodium azide. To get confirmation about the existence of the bonds in both the complexes in the initial stage the FT-IR spectral study of quercetin, complexes 1 & 2 has been carried out and Fig. S1, S2 & S3 in the supporting information file display the IR spectrum of all the stated compounds. Generally, the C=O stretching frequency in free quercetin is seen at 1663 cm^{-1} , which is shifted to 1604 cm^{-1} & 1611 cm^{-1} corresponding to complex 1 and complex 2 respectively. This observation supports the coordination of carbonyl oxygen with metal ions. The C=C stretching frequency of free quercetin is identified at 1604 cm^{-1} , which changes to 1553 cm^{-1} and 1545 cm^{-1} in the case of complex 1 and complex 2 respectively. The C-O-C stretching frequency of free quercetin is recognized at 1251 cm^{-1} , which changes to 1309 cm^{-1} and 1286 cm^{-1} for complex 1 and complex 2 respectively. Magnificently, the IR spectra demonstrate a sharp peak at 2059 cm^{-1} and 2060 cm^{-1} which provide reliable proof concerning the existence of the terminal dicyanamide and azide in complex 1 and 2 respectively. Furthermore, Zn-O and Cu-O stretching vibration bands at 630 cm^{-1} and 631 cm^{-1} respectively assign the development of a metal complex and the non-existence of this band in pure quercetin also validates the formation of the metal complex.

The findings of the UV-vis spectroscopic data of the free quercetin and complex 1 and 2 in DMSO is shown in Fig. S4 (supporting information file). Quercetin shows two major absorption bands at 372 nm and 310 nm assigning B-ring absorption (cinnamoyl system) and A-ring (benzoyl system) respectively. After complexation, a noticeable blue shift alteration at 325 nm (band IV) and 265 nm (band III) of the two spectral positions is observed along with the generation of one additional peak at 470 nm supporting the development of complex 1. On the other hand, for complex 2, the former two peaks appear at 310 nm (band IV) and 275 nm (band III) along with the development of one additional peak at 435 nm, supporting the formation of complex 2.

The electrospray ionization mass spectra (positive mode, m/z up to 1200 amu) of the complexes are recorded in methanolic solutions (Fig. S5 & S6 in the supporting information file). Complex 1 and 2 consist of the abundant peaks at $m/z = 240.9866$ and $m/z = 226.9515$ which can be justified with the molecular formula $[\text{C}_{16}\text{H}_{16}\text{ZnN}_3\text{O}_9\text{K}]^{2+}$ (calculated $m/z = 441.2500$) and $[\text{C}_{16}\text{H}_{15}\text{O}_9\text{CuK}]^{2+}$ (calculated $m/z = 226.7500$) respectively.

2.2. EPR spectral study

The solid-state EPR spectrum for complex 2 has been recorded at room temperature and is pictographically represented in Fig. S7 in the supporting information file. The pictograph displays a sharp-ended feature along with a very small hyperfine splitting. The measured spin Hamiltonian parameters, namely, g_{\parallel} , A_{\parallel} , values ($2.28, 165 \times 10^{-4}\text{ cm}^{-1}$), ensure +2 oxidation state of the metal center. The calculated g_{eff} , g_{\parallel} , g_{\perp} , values are 2.001, 2.28, 2.010. All the results support the existence of the +2-oxidation state of complex 2.

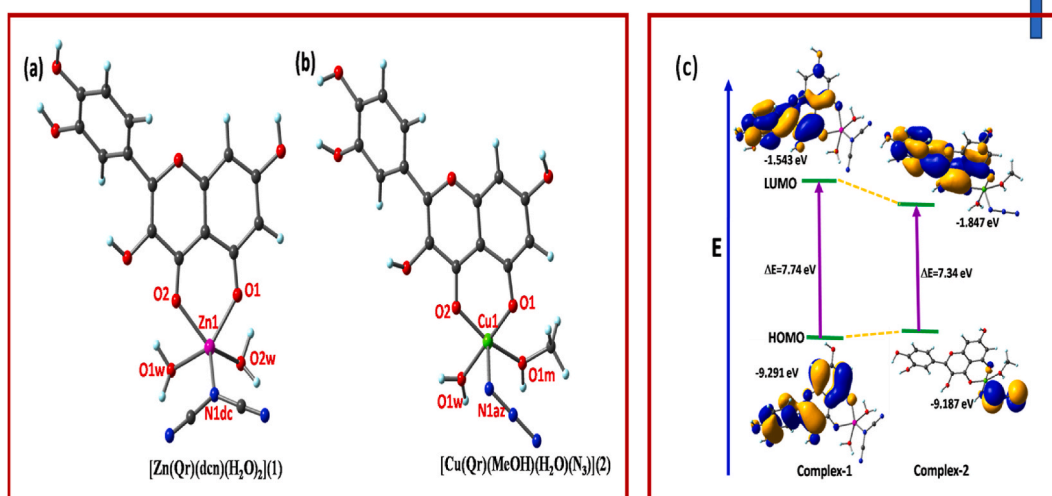


Fig. 1. Geometry optimized molecular structure of (a) 1 and (b) 2 (c) Frontier molecular orbital with an energy difference of complex 1 and 2.

3. Structural optimization through DFT

Following detailed recognition, The DFT investigation assists in structural optimization of two compounds and the DFT-optimized structure of complexes **1** and **2** is displayed in Fig. 1. Before optimization work, the mass spectral data is utilized to confirm the composition of the complexes as $[\text{Zn}(\text{Qr})(\text{NCNCN})(\text{H}_2\text{O})_2](\mathbf{1})$ and $[\text{Cu}(\text{Qr})(\text{MeOH})(\text{H}_2\text{O})(\text{N}_3)](\mathbf{2})$. Table 1 summarizes the.

theoretical parameters associated with complex geometry. The neutral complexes **1** and **2** are penta-coordinated with Zn^{2+} and Cu^{2+} metal centers respectively. complex **1** fulfills the penta coordination geometry by deprotonated bi-dented Qr ligand, one mono-negative dicyanamide anion as secondary anionic residue, and two water molecules. Whereas one deprotonated bidentate Qr molecule, one azide anion as secondary anionic residue and one water and methanol solvent satisfy the coordination forming a pentacoordinate geometry. The Addison parameters are $\tau = 0.006$ and 0.31 for mononuclear complexes **1** and **2** respectively. The theoretical M–N1 bond distance is as 1.915 \AA and 1.860 \AA and M – O bond lengths are ranging as $1.991\text{--}2.191 \text{ \AA}$ and $1.875\text{--}2.020 \text{ \AA}$ for complexes **1** and **2** respectively. The observed HOMO-LUMO energy gap (Fig. 1) are $\Delta E = 7.74 \text{ eV}$ and 7.34 eV for complexes **1** and **2** respectively and this satisfies the stabilization of the complexes.

3.1. DNA binding study

Subsequent confirmation of the structure, the physiological features of the two complexes have been examined in relation to their interactions with HSA and DNA. Prior to proceeding, we first recorded the absorbance spectra of the two complexes as a function of time in the working buffer at pH 7.4 in order to confirm the stability of the complex. The outcome shows that the two concerned metal complexes are extremely stable (Fig. S8 in the supporting information file), with very little variation in their absorption spectra. Following the stability evaluation, the following biophysical analysis is executed to ascertain the complexes' capacity to bind DNA.

3.2. UV absorption titration study

UV-metric titration is a well-established method to understand the binding efficacy of the investigated complexes with DNA. In this experiment, the absorbance changes were recorded after the incremental addition of DNA to a fixed concentration of a target complex. The results unveils that (Fig. 2) after interacting with DNA, in complex **1** the absorption bands in the range $244\text{--}265 \text{ nm}$ and $315\text{--}344 \text{ nm}$ are gradually decreased whereas in complex **2** the absorption band in the range $308\text{--}345 \text{ nm}$ decreases with appearance an isobestic point near at 360 nm . The binding constant can be calculated by implementing the Benesi – Hildebrand (B – H) equation (eq (1)).

$$\frac{1}{A_0 - A} = \frac{1}{(A_0 - A_{\max})K_b \times C} + \frac{1}{(A_0 - A_{\max})} \dots \dots \dots \quad (1)$$

Where A_0 and A refer to the absorbance values of complexes **1** and **2** in the presence and absence of DNA whereas A_{\max} represents the value of absorbance at the saturation of interaction between the investigated complex and DNA. C indicates the concentration of DNA and K_b is the binding constant. The binding constants can be calculated as $5.7 \times 10^4 \text{ M}^{-1}$ and $1.7 \times 10^4 \text{ M}^{-1}$ for complex **1** and **2** respectively. The whole experimental proceedings provide strong proof of the binding efficacy of complexes **1** and **2** with DNA. In a modest comparison, it is found that complex **1** exhibits slightly higher binding efficacy than **2**. This is probably due to the loss of planarity in complex **1** forcing it to bind with DNA via pure groove binding mode whereas complex **2** binds with DNA via partial groove

Table 1
Selective bond distances and bond angles for **1** and **2**.

Bond distance(Å)	M=Zn	M=Cu	Bond angles(°)	M=Zn	M=Cu
M1-N1	1.915	1.860	N1- M1-O1	119.16	106.50
M1-O1	2.055	1.875	N1- M1-O2	122.62	93.80
M1-O2	1.991	1.902	O1- M1-O2	89.29	93.59
M1-O1w	2.191	2.008	O1- M1-O1m	134.51	161.27
M1-O1m/2w	2.189	2.020	O1- M1-O1w	69.53	86.51
			O2- M1-O1m	71.04	86.31
			O2- M1-O1w	134.13	179.87
			N1- M1-O1w	103.10	86.21
			N1- M1-O1m	105.78	92.17

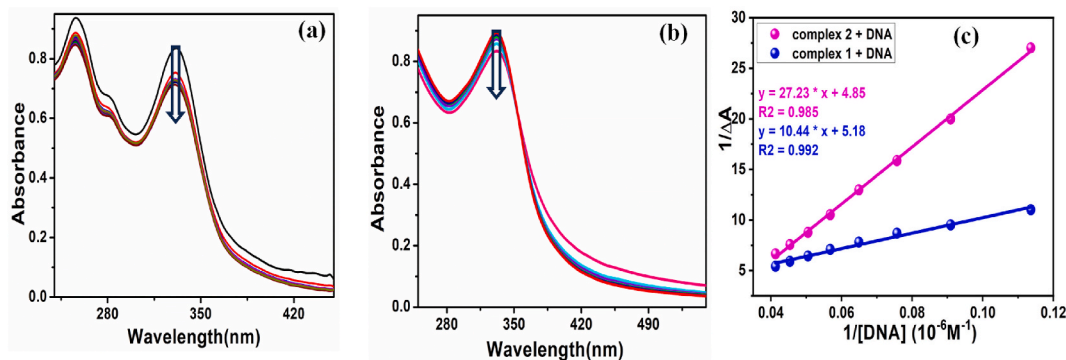


Fig. 2. Change of absorption spectra of (a) complex 1 (15 μM) and (b) complex 2 (15 μM) after incremental addition (2.5–40 μM) of ctDNA to the aqueous buffer solution at pH 7.4. (c) The B – H double reciprocal graph of complex 1 and 2 to determine binding constants for during interaction with DNA.

as well as partial intercalation mode and this partial binding character decreases the binding efficacy of complex 2 than complex 1.

3.3. Fluorescence displacement study

The aforementioned experimental findings make us believers in the binding capability of the complexes with DNA. Now at a glance, it can be seen that the presence of ancillary ligand in the structure of the complexes (dicyanamide moiety in complex 1 and azide moiety in complex 2) is the main reason for the planarity loss in both complexes and due to this signature, it is expected that both the target complexes will favor binding with DNA via groove mode. A thorough structural inspection reveals that the loss of planarity is higher for complex 1 than 2 and this observation provides hints that maybe the groove binding mode will be better for complex 1. To get more insight into the DNA binding interaction of the complexes the fluorescence titration study was performed by using a traditional fluorophore 4',6-diamidino-2-phenylindole (DAPI), which is a recognized groove binder.

In this study initially, DAPI is bound with DNA, and after binding to the DNA, a significant (more than 20-fold) fluorescence intensity enhancement of DAPI can be observed which assure us the strong binding among DAPI and DNA [48,49]. After confirming the saturated binding of DNA with DAPI, the change in Fluorescence intensities of this DNA – DAPI adduct were recorded separately after incremental addition of the complexes in two separate sets. Interestingly from the results it can be seen that (Fig. 3) with separate incremental addition of the complexes to the DNA – DAPI adduct, the fluorescence intensity gradually quenched. In comparison, it is found that the quenching is higher for complex 1 (Fig. 3c) (see Fig. 4).

Using the Stern-Volmer equation (eq (2)), [50].

$$\frac{F_0}{F} = K_q [Q] + 1 \dots\dots\dots (2)$$

The Stern-Volmer quenching constant can be calculated as $1.19 \times 10^5 \text{ M}^{-1}$ and $7.79 \times 10^4 \text{ M}^{-1}$ for complexes 1 and 2 respectively. It can be explained that the replacement of DAPI by the developed complex from the DNA-DAPI adduct releases bare DAPI into the buffer medium and this phenomenon leads to a substantial reduction in fluorescence intensity. As DAPI is a recognized groove binder,

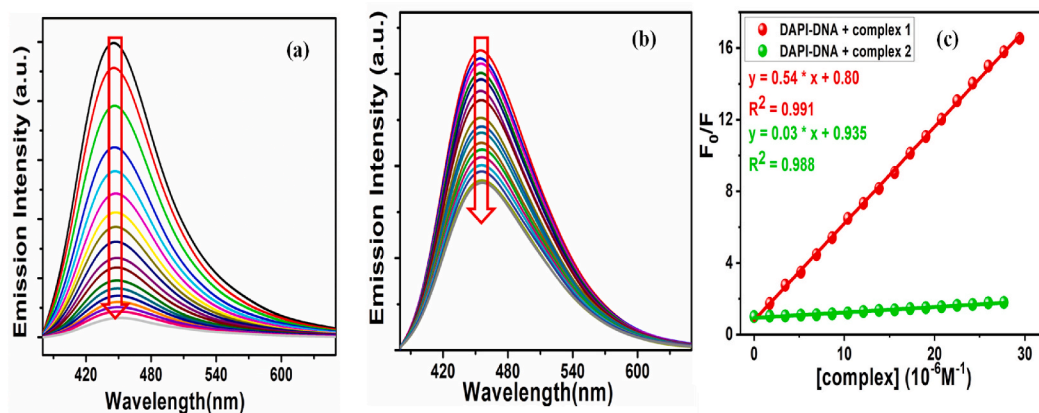


Fig. 3. Fluorescence intensity quenching of DAPI – DNA adduct with the incremental addition of (2.5 μM –40 μM) (a) complex 1 and (b) complex 2. (c) The Stern-Volmer plots of complex 1 and 2 to DAPI -DNA adduct for determining the quenching constants.

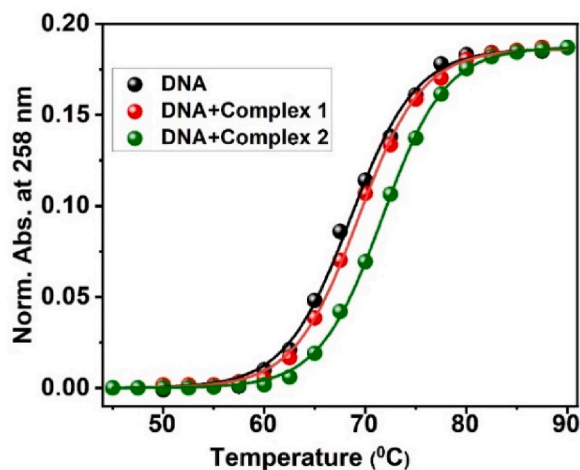


Fig. 4. Thermal melting curves of DNA in the absence and presence of the complexes. [DNA] = 100 μM and [complex] = 10 μM .

this experiment proves that complexes 1 and 2 both can bind with DNA via groove binding mode. However, the quenching ability of complex 1 is found to be higher than that of complex 2, confirmed by the quenching constant value. The bigger space-fill arrangement and high planarity loss character boost it for pure groove binding towards DNA, leading to better binding ability.

3.4. DNA melting study

The groove-binding mode of both the complexes and DNA is further validated by the DNA helix melting experiment. This experiment, upon heating in a controlled path, breaks the hydrogen bonding as well as the base stacking interactions between the strands of the double helix structure of DNA which leads to the conversion of the double strand to single strands structure of DNA [51].

DNA melting temperature (T_m) is considered as the temperature when half of the DNA double-strand is transformed into single strands and in this study, T_m is measured in the absence and in the presence of the complexes [52–54]. Interestingly, the T_m values continuously change with the variation of probe-DNA interaction upon heating. As a measurement parameter, the absorbance of DNA at 260 nm is utilized. In general, When the intercalative binding mode is functioning, the thermal stability of the DNA double helix

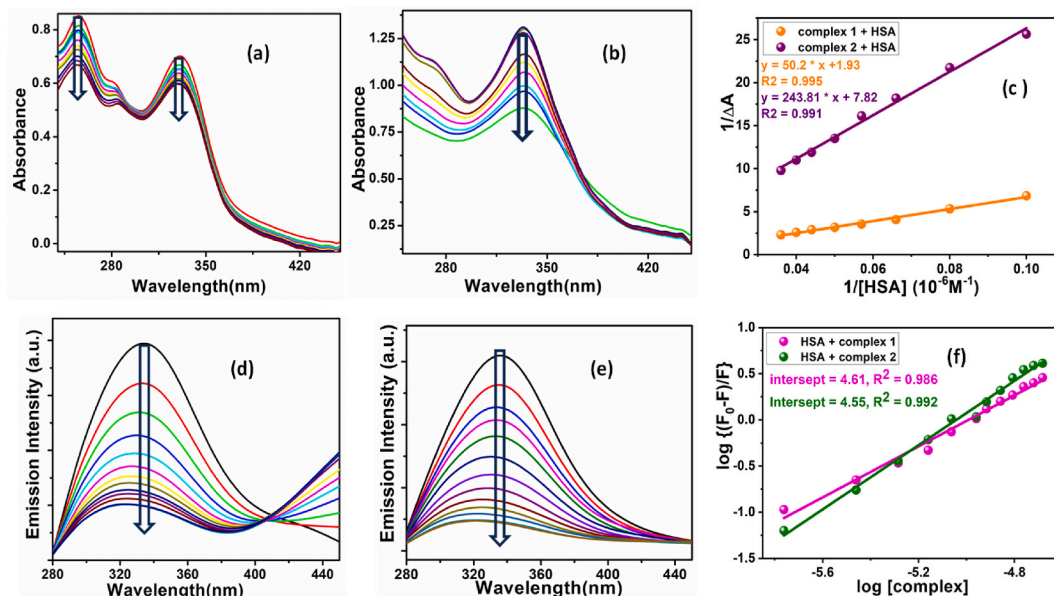


Fig. 5. Absorbance changes of (a) complex 1 (15 μM) and (b) complex 2 (15 μM) after incremental introduction of HSA (2–30 μM). (c) Benesi-Hildebrand double reciprocal plot for complex 1 and complex 2. Fluorescence intensity of 5 μM HSA with increasing concentrations of (d) complex 1 (2.5–40 μM) and (e) complex 2 (2.5–40 μM) at 298 K. (f) Double log plots of Complex 1 and 2 to determine the binding constants during the interaction of HSA with the complex.

structure is increased. That's why T_m value is increased by around 5–8 °C [55–57]. On the other hand, this temperature enhancement is found to be slightly less (2–3 °C) [50] in the case of groove binding. In this experiment we observed that the measured melting temperatures (T_m) for free DNA, DNA-complex 1, and DNA-complex 2 systems' are found to be 68.42 (± 0.2) °C, 74.15 (± 0.2) °C, and 73.12 (± 0.2) °C, respectively. This experiment yields authentic proof about the groove-binding nature of both complexes with DNA.

3.5. Protein binding study

substantial quantity of HSA is present in plasma, where it functions as a drug transporter to transfer drug molecules to the right target regions, reducing the unintended negative effects of the drug molecules. Here, the binding efficiency of both target complexes with this transporter HSA protein has been evaluated using a range of biophysical techniques.

3.6. Spectroscopic investigation

In this study, we adopted all the experiments discussed earlier. But instead of DNA, we tried to investigate the interaction between the investigated complexes with HSA. Here from the UV spectroscopic titration experiment it is observed that with the gradual incorporation of HSA into a fixed concentration of each complex the absorption maxima of the complexes significantly decrease. Fig. 5 pictographically unveils that after the incremental introduction of HSA in complex 1 the absorption maxima in the range of 243–266 nm and 316–342 nm are gradually decreases while in complex 2 the similar observation is noticed in the range of 314–318 nm. This experimental finding demonstrate the effectiveness of the inaction of HSA with both the studied complexes. The isosbestic points on the titration pictograph for the two discussed complexes justify the existence of equilibrium among the free and HSA-bound complexes (Complex 1 and 2). Applying the B–H equation (eq (1)) the binding constant values for protein-complex interaction are listed in Table 2. HSA exhibits strong fluorescent properties due the presence of Tyrosine (Tyr) and tryptophan (Trp), two aromatic amino acid residues as a fluorophore, which are utilized to explain the binding interaction of HSA with investigated drug molecules. Here, in the fluorescence titration experiment after the subsequent addition of each complex separately into HSA at a given concentration, the fluorescence intensity of HSA at around 340 nm is significantly quenched, as shown in Fig. 5.

This observation is a strong indication of HSA-complex binding. The binding constants for the two HSA-complex adducts (Fig. 6) have been determined using the double-log equation (eq (3)), and the results are summarized in Table 2.

$$\log \frac{F_0 - F}{F} = \log K_b + n \log [Q] \dots \dots \dots (3)$$

For the HSA–complex conjugates, Temperature-dependent binding experiments are conducted (Fig. 6), and the analysis of the results reveals that the binding constant values are directly proportional to the temperature changes (Table 3) [58]. We have applied equation (4) (eq (4)) to the determine the value of ΔH and ΔS ($\Delta H > 0$, $\Delta S > 0$), and these values proclaim a significant information that the interaction is ruled by hydrophobic force [59,60].

$$\ln K_b = -\frac{\Delta H^0}{RT} + \frac{\Delta S^0}{R} \dots \dots \dots (4)$$

Finally, the spontaneous interaction among complexes and HSA is confirmed by negative free energy change.

3.7. Circular dichroism study

The approach preference to find out whether or not the biomacromolecules suffer any secondary conformational changes during their interactions with the title complexes, circular dichroism (CD) spectral titration was carried out. The CD spectra of bare DNA and HSA are first recorded in this measurement. Then, following the addition of complexes 1 and 2 in a dose-dependent manner, the changes in the CD spectra of the biomacromolecules are meticulously documented. Fig. 7 displays the experimental finding of the CD titration results. The canonical B form of DNA is supported by the CD spectrum of free DNA, which can be seen in the photograph as it exhibits a positive lobe at 276 nm and a negative lobe at 243 nm. Interestingly it is observed that no discernible change in spectral character appears upon the association of each complex with DNA whereas only the lobe depth varies very little. This result indicates

Table 2
Binding parameters of HSA with complex 1 and 2.

Sample	From absorption study		From fluorescence study	
	$K_b \times 10^4$ (L mol ⁻¹)		$K_b \times 10^4$ (L mol ⁻¹)	n
HSA-complex 1	3.85		4.07	0.99
HSA-complex 2	3.23		3.54	1.08

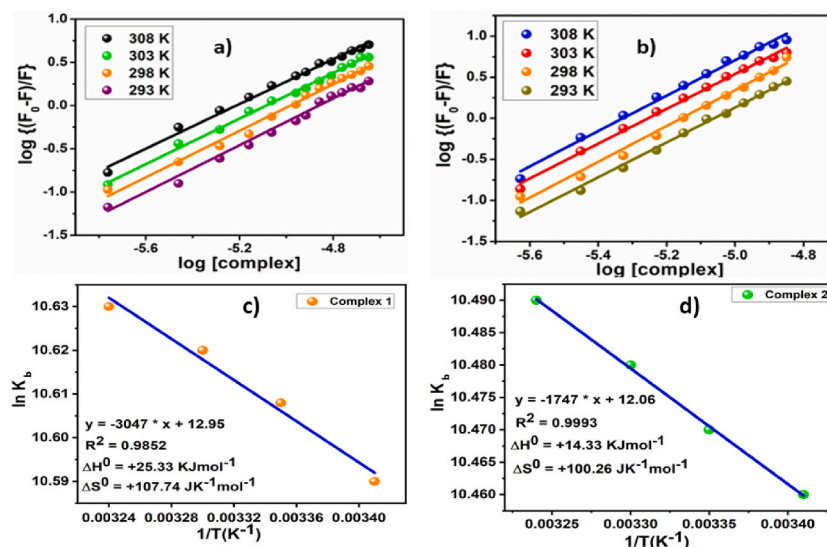


Fig. 6. Double log plot of HSA with varying temperatures for (a) complex 1 and (c) complex 2. Van't Hoff plots during the interaction of HAS with (b) complex 1 and (d) complex 2.

Table 3

Binding constant alteration (K_b) of HSA during association with complex 1 and 2 with temperature changes.

Complexes	Temperature (K)	K_b Values
Complex 1	293	3.98×10^4
	298	4.07×10^4
	303	4.11×10^4
	308	4.14×10^4
Complex 2	293	3.50×10^4
	298	3.54×10^4
	303	3.59×10^4
	308	3.62×10^4

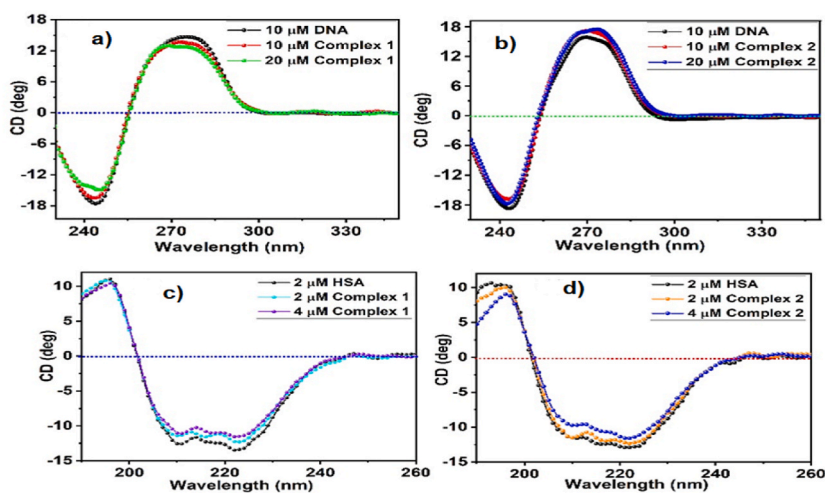


Fig. 7. CD spectral changes of ctDNA in the absence and presence of (a) complex 1 and (b) complex 2. CD spectral changes of HSA in the absence and presence of (c) complex 1 and (d) complex 2.

that a significant amount of the DNA configuration is maintained when interacting with the complexes being studied.

On the other hand, HSA exhibits two negative peaks at 208 and 222 nm offers confirmation for the helical shape of the macromolecule. The CD spectral nature of HSA in the current study differs slightly when target complexes are present (Fig. 7), and this observation suggests that the developed complexes have some ability to alter the structure of the protein.

3.7.1. Molecular docking study

Molecular docking study gives important information in understanding the binding interactions of small biologically active molecules with biological macromolecules such as DNA, protein etc. [61–63]. In the present study following a successful experimental investigation of the binding interactions of the two complexes with ctDNA and HSA, the precise binding locations and active binding sites of the probe inside the macromolecules have been theoretically interpreted using Auto Dock Vina program (see experimental section). The scoring function in Auto Dock Vina (measured in kJ mol⁻¹) is utilized to estimate the predicted binding affinity between a ligand and its receptor, assessing the strength of the binding interaction between the two molecules. The scoring function is influenced by both conformation-dependent factors (intra- and intermolecular contributions, steric, hydrophobic, and hydrogen bonding interactions) and conformation-independent factors (rotatable bonds present in ligands) [64,65]. The docking calculations on the complex-DNA system provide clear evidence that, for the most stable conformer, both complexes bind to the minor groove region of the DNA helix (Fig. 8). The groove binding mechanism is primarily driven by strong hydrogen bonding between the ligand complexes and nucleic acid bases. The computed docking energies for the most stable docked conformations are -43.26 kJ/mol for complex 1 and -35.28 kJ/mol for complex 2, exhibiting a similar trend to the experimental complex-DNA binding constants mentioned above.

The higher binding affinity of complex 1 towards DNA can be attributed to the formation of additional hydrogen bonds relative to complex 1. This existence of extra hydrogen bonds is believed to contribute to a stronger interaction between the complex and the DNA molecule. Fig. 8 gives strong evidence that the orientation of the ligand in complexes significantly influences the binding affinity of the target complexes with DNA.

Regarding serum protein binding, molecular docking calculations suggest that both complexes bind to the sub-domain IB of the HSA protein through a combination of hydrogen bonding and hydrophobic interactions (Fig. 9). The docked binding energies for the complexes 1-HSA and complex 2-HSA interaction are determined as -42.8 kJ/mol and -40.7 kJ/mol, respectively. Interestingly, these theoretical observations not only align with the experimental binding constant values but also demonstrate a close proximity between the two numerical values, which shows different behavior, observed during DNA binding. During interaction with HSA, similar orientation exhibited by both the complexes is mainly the responsible factor for giving close binding constant values during interaction of target complexes with HSA. However, complex 1 forms an additional hydrogen bond in comparison to complex 2, resulting in a slightly enhanced of binding affinity. Therefore, consistent with other spectroscopic studies, the molecular modeling further corroborates the proposition of groove binding interactions between complexes with ctDNA, as well as their binding affinity towards serum protein.

3.8. Antioxidant property

By employing a UV–vis spectrophotometer and the stable DPPH molecule, the antioxidant activity of quercetin and its two studied

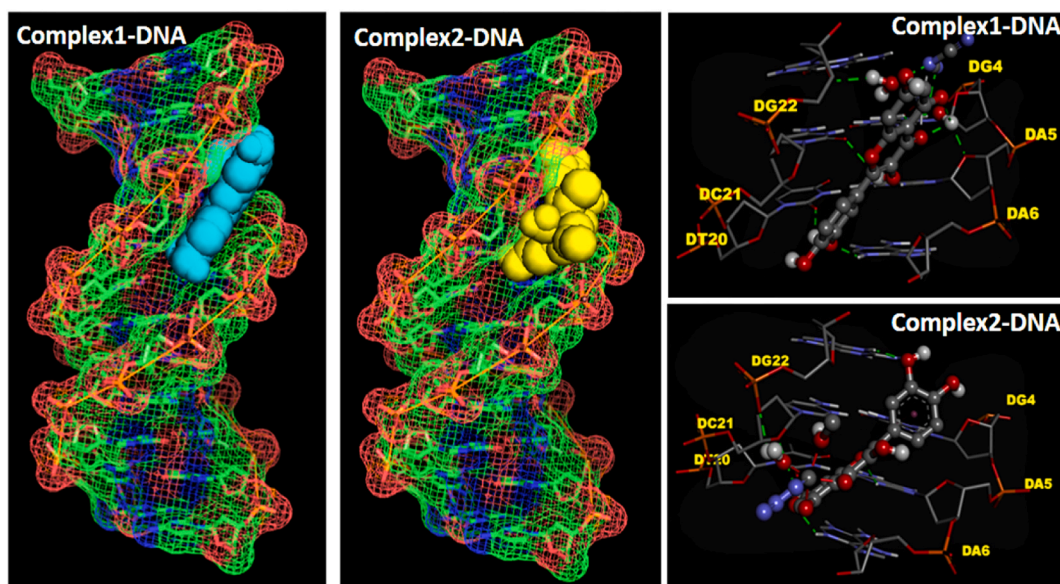


Fig. 8. Minimum energy molecular docked conformations of complex 1 and 2 with the DNA and binding interactions between complexes and DNA (green dotted lines represent H-bonding between these two).

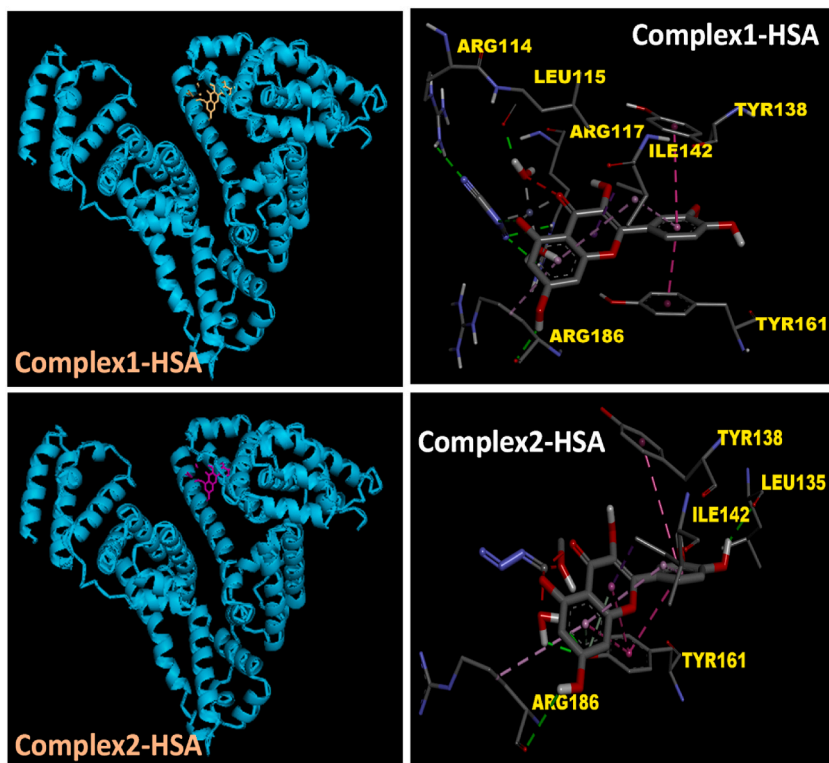


Fig. 9. Minimum energy molecular docked conformations of complex 1 and 2 with the HSA and binding interactions between ligands and HSA protein (green dotted lines represent H-bonding between these two).

complexes have been assessed in terms of its hydrogen-donating or radical-scavenging capacity. The maximum absorption at 517 nm (purple colour) results from the interaction of a free radical of DPPH with an odd electron. The reaction between DPPH and a free-radical scavenger antioxidant produces DPPHH, which has a lower absorbance than DPPH due to the lower hydrogen content. This radical form exhibits decolorization (a yellow hue) in comparison to the DPPH-H state due to the enhancement of gathered electrons. The results of the experiment are pictographically summarized in Fig. 10 and Fig. S9 (In the supporting information file). It can be observed that at a fixed concentration, complex 1 has the highest antioxidant property than Complex 2 as well as Qr. The percentage of antioxidant activity can be calculated as 78.31 %, 58.40 %, and 32.58 % for complex 1, 2 and Qr respectively.

It is well known that quercetin shows significant DNA/protein binding and antioxidant activity but when it forms a complex with different metal ions then the antioxidant property as well as the binding efficacy of the macromolecules readily increases [66–71]. Here interestingly the binding ability towards macromolecules and the antioxidant property of the metal-quercetin complex with the presence of ancillary ligand is comparable with the simplex quercetin-metal complex.

3.9. *In-vitro* cytotoxicity assay

Following the DNA and HSA binding efficacy testing, the MTT assay is used to verify the cytotoxicity experiment of both target complexes on the HEK 293 normal cell line and the HeLa cancer cell line in a dose-dependent manner. The results of the cell viability studies are summarized in Fig. 11. After both cells are incubated for 24 h at different dosages of the two complexes, the IC₅₀ values have been determined. Cisplatin has been utilized as a positive control against the HeLa cell line (IC₅₀ = 14.7) for the entire MTT test [72].

The IC₅₀ values for complex 1 (displayed in Table 4) provide strong evidence for potent anticancer ability with low toxicity to normal cells confirms by its high IC₅₀ value for normal cells. On the other hand the large IC₅₀ value for compound 2 for HeLa cells indicates that it is unable to demonstrate any meaningful anticancer effects. In this case, it's important to remember that Zn- or Cu-quercetin complexes have also shown anticancer effects in the past, but there's no evidence to suggest that the complex has less of an impact on normal cells [73,74].

4. Conclusion

One Zn(II) complex based on quercetin, called Zn(Qr)(CNNCN)(H₂O)₂, (complex 1) has been developed in recent work by a simple condensation reaction between quercetin and zinc chloride in the presence of NaN(CN)₂, and one Cu(II) complex, called Cu(Qr)N₃

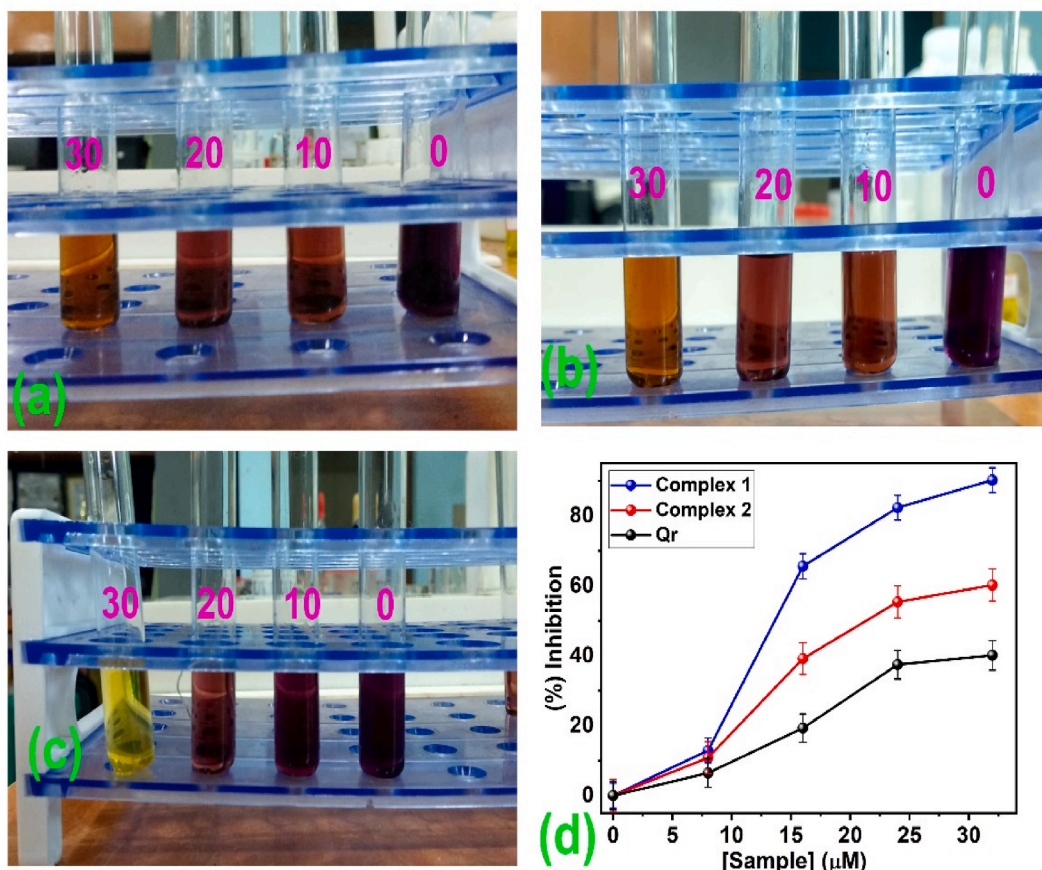


Fig. 10. Optical colour change of DPPH in addition to different concentrations of (a) Quercetrin (b) Complex 1 (c) Complex 2 and (d) Plot of [sample] vs % of Inhibition to calculate the antioxidant activity.

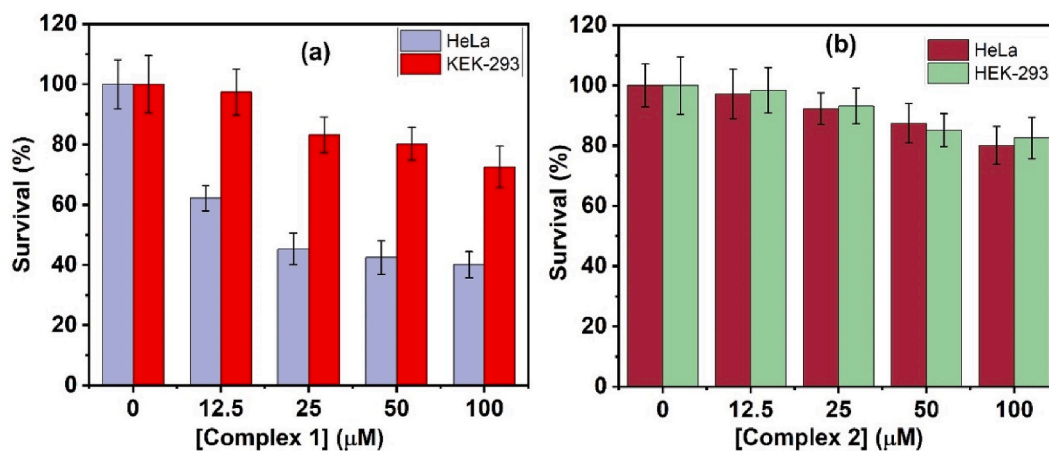


Fig. 11. Cell viability of HeLa cell line after incubation with complex 1 via dose dependent manner for a) 24 h b) 48 h.

(H₂O)(MeOH) (complex 2), has been formed through a reaction between and CuCl₂ in the presence of sodium azide. Newly developed complex 1 and 2 are properly identified via numerous spectroscopic techniques. EPR analysis verifies that the metal oxidation state in complex 2 is + 2. DFT analysis is used to determine the two complexes' optimized structures. After precise identification, both complexes are subjected to a battery of biophysical tests, including UV metric, fluorometric, and CD titration, as well as DNA melting, to assess their DNA and HSA binding ability. The results of every biophysical investigation confirm that the complexes with DNA and

Table 4
IC50 value of the target compounds.

Compounds	HeLa (μM) (24 h incubation)	HEK 293 (μM) (24 h incubation)
Complex 1	31.25 ± 2.92	86.1 ± 3.49
Complex 2	>100	>100
Cisplatin (Reference)	14.7 ± 1.2	

HSA have substantial binding efficacies. But, complex 1 has better susceptibility for effective binding with the macromolecules due to the presence of an additional H-bond during interaction with HSA and the operation of pure groove binding mode in the time of association with DNA. The thermodynamic parameter measuring further validates the spontaneous binding of the investigated compounds with HSA. Finally, the antioxidant and cancer-fighting abilities of these complexes have been investigated. The lower IC50 value for HeLa cell and higher IC50 value for normal HEK cell approve effective anticancer properties of complex 1 with little toxicity to normal cells. Better DNA and HSA binding ability of complex 1 may play a key role in exhibiting strong anticancer properties. Remarkably, complex 1's antioxidant properties surpass both quercetin and complex 2, indicating a potential enhancement of the quercetin-metal complex's bioapplication properties when an ancillary ligand is present.

5. Experimental section

5.1. Materials and methods

There was no need for further purification because all of the reagents and solvents utilized in the synthetic process were readily accessible on the market as reagent-grade compounds. We purchased EB, DAPI, HSA, and CT-DNA from Sigma Aldrich Chemicals. Merck provided the quercetin hydrate, zinc chloride, copper chloride, sodium azide, sodium dicyanamide ($\text{NaN}(\text{CN})_2$), and triethylamine (Et_3N). A PerkinElmer 2400II elemental analyzer was utilized in the current investigation to conduct elemental (C, H, and N) analysis. A Bruker Tensor-27 in ATR mode was used to obtain FTIR data. PerkinElmer UV-VIS Lambda 365 spectrophotometer was utilized for the electronic absorption experiments, while PerkinElmer FL6500 fluorescence spectrophotometer was used for the fluorometric measurements. The total interaction investigations among macromolecules and complexes were executed in citrate-phosphate (CP) buffer of 10 mM $[\text{Na}^+]$ at pH 7.4 containing 0.5 mM Na_2HPO_4 .

5.2. Synthetic procedures

Synthesis of $[\text{Zn}(\text{Qr})(\text{MeO})(\text{H}_2\text{O})\text{N}(\text{CN})_2]$ (5)

For the synthesis of complex 1, the methanolic solution of 0.136 g (1 mmol) ZnCl_2 was added in situ to the methanolic solution of 0.30 g (1 mmol) quercetin under reflux conditions with continuous stirring followed by addition of 0.089 g (1 mmol) $\text{NaN}(\text{CN})_2$. The mixture was then stirred for 3 h. The yellow colored ppt appeared during the complex 1 generation. After that, the solution was left at room temperature to settle and filtered. The ppt was collected and dried for further studies. Yield: 85 %.

Anal. Calc.: For $\text{C}_{18}\text{H}_{14}\text{N}_3\text{O}_9\text{Zn}$ (MW: 481.70) C, 44.68; H, 2.73; N, 8.52; Found C, 44.88; H, 2.93; N, 8.72.

Synthesis of $[\text{Cu}(\text{Qr})(\text{MeO})(\text{H}_2\text{O})\text{N}_3]$ (6)

During complex 2 preparation, we followed the same synthetic procedure as complex 1. Here instead of ZnCl_2 we have used CuCl_2 and instead of $\text{NaN}(\text{CN})_2$ we have used NaN_3 . Here we got brown colored ppt appeared during the complex 2 generation. Yield: 85 %.

Anal. Calc.: For $\text{C}_{16}\text{H}_{14}\text{N}_3\text{O}_9\text{Cu}$ (MW: 455.85) C, 41.96; H, 2.90; N, 9.02; Found C, 42.16; H, 3.10; N, 9.22.

5.3. Theoretical calculation method

Ground-state electronic structure measurements in the gas phase of the ligand and complex have been worked out using a DFT procedure attached to the conductor-like polarizable continuum model [75] Becke's hybrid function [76] with the Lee–Yang–Parr [77] correlation function was used for the exploration. The absorbance spectral characteristics in the DMSO medium for complexes 1 & 2 were reckoned by time-dependent density functional theory, attached with the conductor-like polarizable continuum model and we measured the lowest 40 singlet–singlet transition.

For H atoms, we applied the 6–31+(g) basis set; for C, N, O, Zn and Cu atoms, we utilized LanL2DZ as the basis set for all the measurements. The determined electron-density plots for frontier molecular orbitals were prepared by using Gauss View 5.1 software. By using the Gaussian 09 W software package the total measurements were done. The Gauss Sum 2.1 program [78] was used to determine the molecular orbital contributions from groups or atoms.

5.4. DNA/protein interaction studies

The DNA and HSA stock solution were set up by dissolution of CT-DNA in a CP buffer of 10 mM Na^+ containing 0.5 mM Na_2HPO_4 .

The DNA concentration was ascertained spectrophotometrically using the molar extinction coefficient (ϵ) $6600 \text{ M}^{-1} \text{ cm}^{-1}$, and no dislocation from Beer's law was detected during concentration estimation. Simultaneously, a certain concentration of HSA was prepared by appointing the molar extinction coefficient (ϵ) of $37,500 \text{ M}^{-1} \text{ cm}^{-1}$. The subsequent biophysical studies were accomplished to assess the binding efficacy of DNA/protein with complexes **1** and **2**.

5.5. Circular dichroism spectral study

Circular dichroism (CD) spectral studies were carried out utilising a JASCO J815 model unit (JASCO International Co. Ltd. Hachioji, Japan) outfitted with a JASCO temperature controller (PFD 425L/15). Enhancing concentrations of complex **1** and **2** were added to a certain concentration of CT-DNA or HSA to perform titrations. Documentation was done of the changes in the free DNA/HSA CD spectrum following the inclusion of the complexes. The equation was utilized to compute the molar ellipticity values $[\theta]$ in the DNA interaction investigations.

$$[\theta] = 100 \times \theta / (C \times l) \quad (7)$$

where θ is the noticed ellipticity in millidegrees, C is the concentration in mol/L, and l is the cuvette cell path length in cm. The molar ellipticity $[\theta]$ ($\text{deg. cm}^2/\text{dmol}$) values within the region of 200–400 nm are illustrated in terms of base pairs [79,80]. For the HSA interaction study in 190–260 nm wavelength region, the CD scans were performed. The executed ellipticity (θ) was explicated as:

$$\text{MRE} = \theta M / a c l \quad (8)$$

where M stands for the molar mass of the protein, a describes the number of amino acids in the protein, c shows the concentration in g L^{-1} , and l is the path length.

5.6. Molecular modeling studies for DNA binding and HSA protein interaction

Molecular docking calculations were performed using AutoDock Vina program (version 1.1.2) in conjunction with the Autodock Tools from the Scripps Research Institute [81]. The structures of Zn-based Complex **1** and Cu-based Complex **2** were initially obtained from their crystallographic data in CIF file format. These CIF files were then converted into PDB files using Open Babel GUI software. The macromolecular crystal structures of calf thymus DNA (ctDNA) and Human Serum Albumin (HSA) were obtained from the RCSB Protein Data Bank (widely accepted database for biological research) having PDB ID 1BNA (B-DNA, d(CGCGAATTCGCG)₂ dodecamer) and 2I2Z respectively. AutoDock Vina offers superior accuracy compared to AutoDock 4 docking software in predicting the binding affinity of the probe/drug towards the biomolecule [82]. The PDB files of the receptor/s (DNA and HSA) and ligand complexes (**1** and **2**) were then converted into PDBQT format using the MGL Tool (version 1.5.6) prior to conducting the docking studies. A sufficiently large three dimensional grid box of $100 \times 100 \times 100$ was created with a grid spacing 0.375 \AA (for DNA) and 1.00 \AA (for HSA), encompassing the entire macromolecules and allowing the complexes to explore all potential binding sites of biomolecules. Docking calculations were conducted using a generic algorithm run of 20 iterations, an exhaustiveness value of 8, and an energy range of 4. Finally, according to the Autodock scoring function, the lowest energy conformer of complex-macromolecular adduct was selected as the most stable conformation. PyMOL and BIOVIA Discovery Studio Visualizer software package were employed for visualization and analysis of the docked conformations. These software tools are widely used in the field of biophysical chemistry for their robust features and capabilities in analyzing the receptor-ligand interactions.

5.7. Antioxidant property experiment of the complexes by DPPH method

To assess the free radical scavenging abilities of the complexes **1**, 1,1-diphenyl- 2-picryl hydrazyl (DPPH) technique was implemented [83]. 100 ml stock solution of DPPH was freshly prepared by dissolving 24 mg of the sample into 100 ml methanol. Then 0.1 ml of different concentrations of complexes (8, 16, 24, and 32 μM) were added into 3.9 ml of DPPH solution (100 μM) and mixed gently. Then it is kept in a dark room for about 30 min. A blank solvent as a sample was used as a control. After that, the absorbance change of DPPH was recorded at 517 nm. To get accurate results this experiment was repeated 3 times. To calculate the percentage of antioxidant activity the following equation (equa ... 6) has been used [84].

$$\% \text{ of antioxidant activity} = [(A_c - A_s) \div A_c] \times 100 \quad (9)$$

where: A_c is the absorbance of Control during the reaction; A_s is the absorbance of the sample mixture during the reaction.

5.8. In vitro cytotoxicity assay study

The traditional MTT test method was used to assess the anticancer activity of the examined complexes on the human cervical carcinoma (HeLa) cell line and the HEK 293 normal cell line. In a 24-well plate, each cell was seeded at a density of 2×10^5 cells/well. Cells were exposed to the aforementioned complexes for 24 and 48 h at various doses following a 24-h cell seeding period. After incubation, cells were twice rinsed with 1X phosphate buffered saline (PBS). They were then exposed to 0.5 mg/mL MTT solution (SRL) and allowed to incubate for a further 3–4 h at 37°C until the formation of a purple formazan product. The outcome product was then dissolved in DMSO and finally with the aid of a microplate reader (Bio-Rad) at 570 nm OD was determined. The following formula was

applied to calculate the rate of survival.

$$\text{Cell viability (\%)} = (\text{OD}_{\text{AT}} / \text{OD}_{\text{AC}}) \times 100 \quad (10)$$

where OD_{AT} = Absorbance of control cells and OD_{AC} = Absorbance of treated cells [85].

Data availability statement

Data will be made available on request.

CRediT authorship contribution statement

Anupam Mudi: Methodology. **Shubham Ray:** Data curation. **Manjushree Bera:** Methodology. **Malay Dolai:** Validation. **Manik Das:** Software, Formal analysis. **Pronab Kundu:** Software. **Soumik Laha:** Formal analysis, Data curation. **Indranil Choudhuri:** Methodology. **Bidhan Chandra Samanta:** Data curation. **Nandan Bhattacharyya:** Formal analysis. **Tithi Maity:** Writing - original draft, Supervision, Investigation, Conceptualization.

Declaration of competing interest

There are no conflicts of interest to mention.

Acknowledgments

The corresponding author (TM) thanks to the administration of Prabhat Kumar College, Contai for their ongoing assistance. TM is grateful to the West Bengal government's Department of Science & Technology and Biotechnology for the funding provided under the Gobeshonay Bangla Scheme. Additionally, TM thanks DST FIST for providing financial support to the College.

Appendix A. Supplementary data

Supplementary data to this article can be found online at <https://doi.org/10.1016/j.heliyon.2023.e22712>.

References

- [1] G.F. Weber, Mol. Cancer Therapeut. (2014) 8–12.
- [2] B.J. Pages, D.L. Ang, E.P. Wright, J.R. Aldrich-Wright, Metal complex interactions with DNA, Dalton Trans. 44 (2015) 3505–3526.
- [3] A.C. Komor, J.K. Barton, The path for metal complexes to a DNA target, Chem. Commun. 49 (2013) 3617–3630.
- [4] C.-Y. Zhou, J. Zhao, Y.-B. Wu, C.-X. Yin, P. Yang, Synthesis, characterization and studies on DNA-binding of a new Cu(II) complex with N^1, N^8 -bis(1-methyl-4-nitropropyl-2-carbonyl)triethylenetetramine, J. Inorg. Biochem. 101 (2007) 10–18.
- [5] A.-M. Florea, D. Busselberg, Cisplatin as an anti-tumor drug: cellular mechanisms of activity, drug resistance and induced side effects, cancer 3 (1) (2011) 1351–1371.
- [6] L. Qi, Q. Luo, Y. Zhang, F. Jia, Y. Zhao, F. Wang, Advances in toxicological research of the anticancer drug cisplatin, Chem. Res. Toxicol. 32 (8) (2019) 1469–1486.
- [7] J.-L. Juo, G.-Y. Liu, R.-Y. Wang, S.X. Sun, Synthesis and structure elucidation of two essential metal complexes: in-vitro studies of their BSA/HSA-Binding properties, docking simulations, and anticancer activities, Molecules 27 (6) (2022), 1886.
- [8] D.-H. Cai, B.-H. Chen, Q.-Y. Liu, X.-Y. Le, L. He, Synthesis, structural studies, interaction with DNA/HAS and antitumor evaluation of new Cu(II) complexes containing 2-(1H-imidazole-2-yl)pyridine and amino acids, Dalton Trans. 51 (2022) 16574–16586.
- [9] J. Zhang, X. Gao, J. Huang, H. Wang, Probing the interaction between human serum albumin and 9-hydroxyphenanthrene: a spectroscopic and molecular docking study, ACS Omega 27 (5) (2020) 16833–16840.
- [10] S. Siddiqui, F. Ameen, S.U. Rehman, T. Sarwar, M. Tabis, Studying the interaction of drug/ligand with serum albumin, J. Mol. Liq. 336 (2021), 116200.
- [11] A. Rauf, M. Imran, I.A. Khan, M.-U. Rehman, S.A. Gilani, Z. Mehmood, M.S. Mubarak, Anticancer potential of quercetin: a comprehensive review, Phytother Res. 32 (11) (2018) 2109–2130.
- [12] E. Middleton, C. Kandaswami, T.C. Theoharides, The effects of plant flavonoids on mammalian cells: implications for inflammation, heart disease, and cancer, Pharmacol. Rev. 52 (2000) 673–751.
- [13] J. Haslam, Natural polyphenols (vegetable tannins) as drugs: possible modes of action, J. Nat. Prod. 59 (1996) 205–215.
- [14] J.B. Harborne, C.A. Williams, Advances in flavonoid research since 1992, Photochemistry 55 (2000) 481–504.
- [15] P.C.H. Hollman, M.B. Katan, Dietary flavonoids: intake, health effects and bioavailability, Food Chem. Toxicol. 37 (1999) 937–942.
- [16] D. Prochazkova, I. Bousova, N. Wilhelmova, Antioxidant and prooxidant properties of flavonoids, Fitoterapia 82 (2011) 513–523.
- [17] T.P.T. Cushnie, A.J. Lamb, Recent advances in understanding the antibacterial properties of flavonoids, Int. J. Antimicrob. Agents 38 (2011) 99–107.
- [18] D.M. Kopustinskiene, V. Jakstas, A. Savickas, J. Bernatoniene, Flavonoids as anticancer agents, Nutrients 12 (2020) 457.
- [19] M. Yamaguchi, T. Murata, B.F. EL-Rayes, M. Shoji, The flavonoid p-hydroxycinnamic acid exhibits anticancer effects in human pancreatic cancer MIA PaCa-2 cells in vitro: comparison with gemcitabine, Oncol. Rep. 34 (2015) 3304–3310.
- [20] M. Cardenas, M. Marder, V.C. Blank, L.P. Roguin, Antitumor activity of some natural flavonoids and synthetic derivatives on various human and murine cancer cell lines, Bioorg. Med. Chem. 14 (9) (2006) 2966–2971.
- [21] F.L. Chan, H.L. Choi, Z.Y. Chen, P.S. Chan, Y. Huang, Induction of apoptosis in prostate cancer cell lines by a flavonoid, baicalin, Cancer Lett. 160 (2) (2000) 219–228.
- [22] S. Kawaii, Y. Tomono, E. Katase, K. Ogawa, M. Yano, Antiproliferative activity of flavonoids on several cancer cell lines, Biosci. Biotechnol. Biochem. 63 (5) (1999) 896–899.

- [23] A. Bisol, P.S.D. Campos, M.L. Lamers, Flavonoids as anticancer therapies: A systematic review of clinical trials, *phytotherapy Research* 34 (2020) 568–582.
- [24] J.G. Jakubowicz, R. Paduch, T. Piersiak, T. Głowniak, A. Gawron, M. Kandefer Szerszen, *Biochem. Pharmacol.* 69 (2005) 1343–1350.
- [25] S. Ramos, Effects of dietary flavonoids on apoptotic pathways related to cancer chemoprevention, *J. Nutr. Biochem.* 18 (2007) 427–442.
- [26] M. Das, S. Mukherjee, M.M. Islam, I. Chaudhuri, N. Bhattacharya, B.C. Samanta, B. Dutta, T. Maity, Response of ancillary azide ligand in designing a 1D copper (II) polymeric complex along with the introduction of high DNA- and HAS-binding efficacy, leading to impressive anticancer activity: a compact experimental and theoretical approach, *ACS Omega* 7 (2022) 23276–23288.
- [27] K.M. Oliveira, J. Honorato, G.R. Goncalves, M.R. Cominetti, A.A. Batista, R.S. Correa, Ru(II)/diclofenac-based complexes: DNA, BSA interaction and their anticancer evaluation against lung and breast tumor cells, *Dalton Trans.* 49 (2020) 12643–12652.
- [28] Y. Li, Y. Li, Z. Yang, F. Meng, M. Jhou, Z. Xia, Q. Gong, Q. Gao, Distinct supramolecular assemblies of Fe(III) and Ni(II) complexes constructed from the o-vanillin salicylhydrazone ligand: syntheses, crystal structures, DNA/protein interaction, and antioxidant and cytotoxic activity, *New J. Chem.* 43 (2019) 8024–8043.
- [29] Y. Li, Y. Li, N. Wang, D. Lin, X. Lu, Y. Yang, Q. Gao, Synthesis, DNA/BSA binding studies and *in vitro* biological assay of nickel(II) complexes incorporating tridentate aroylhydrazone and triphenylphosphine ligands, *J. Biomol. Struct.* 38 (2020) 4977–4996.
- [30] Y. Li, C. Qian, Y. Li, Y. Yang, D. Lin, X. Liu, C. Chen, Syntheses, crystal structures of two Fe(III) Schiff base complexes with chelating o-vanillin aroylhydrazone and exploration of their bio-relevant activities, *J. Inorg. Biochem.* 218 (2021), 111405.
- [31] M. Bera, M. Das, M. Dolai, S. Laha, M.M. Islam, B.C. Samanta, A. Das, I. Choudhuri, N. Bhattacharyya, T. Maity, DNA/Protein binding and apoptotic-induced anticancer property of a first time reported quercetin-iron(III) complex having a secondary anionic residue: a combined experimental and theoretical approach, *ACS Omega* 8 (2023) 636–647.
- [32] P. Mondal, A. Bose, Spectroscopic overview of quercetin and its Cu(II) complex interaction with serum albumins, *Bioimpacts* 9 (2019) 115–121.
- [33] J. Tan, B. Wang, L. Zhu, DNA binding, cytotoxicity, apoptotic inducing activity, and molecular modeling study of quercetin zinc(II) complex, *Bioorg. Med. Chem.* 17 (2009) 614–620.
- [34] J. Tan, L. Zhu, B. Wang, DNA binding and cleavage activity of quercetin nickel(II) complex, *Dalton Trans.* (2009) 4722–4728.
- [35] S.B. Bukhari, S. Memon, M.M. Tahir, M.I. Bhangar, Synthesis, characterization and investigation of antioxidant activity of cobalt-quercetin complex, *J. Mol. Struct.* 892 (2008) 39–46.
- [36] S.B. Bukhari, S. Memon, M.M. Tahir, M.I. Bhangar, Synthesis, characterization and antioxidant activity copper-quercetin complex, *Spectrochim. Acta. A. Mol. Biomol. Spectrosc.* 71 (2009) 1901–1906.
- [37] S. Jana, R.C. Samanta, S. Das, S. Chattopadhyay, Variation in DNA binding constants with a change in geometry of ternary copper(II) complexes with N₂O donor Schiff base and cyanate or dicyanamide, *J. Mol. Struct.* 1074 (2014) 703–712.
- [38] S.P. Devi, N.S. devi, L.J. Singh, R.K.B. Devi, W.R. Devi, C.B. Singh, R.K.H. Singh, Spectroscopic and DNA interaction studies on mixed ligand copper(II) complexes of dicyanamide with ethylenediamine or 1,3-diaminopropane, *Inorg. Nano-met.* 47 (2017) 223–233.
- [39] M. Das, S. Mukherjee, M.M. Islam, I. Chaudhuri, N. Bhattacharya, B.C. Samanta, B. Dutta, T. Maity, Response of ancillary azide ligand in designing a 1D copper (II) polymeric complex along with the introduction of high DNA- and HAS-binding efficacy, leading to impressive anticancer activity: a compact experimental and theoretical approach, *ACS Omega* 7 (2022) 23276–23288.
- [40] R.K.B. Devi, S.P. Devi, R.K.H. Sing, Synthesis, characterization and DNA interaction study of a new oxovanadium (IV) complex containing acetylacetone and dicyanamide as ligands, *Spectrosc. Lett.* 45 (2012) 93–103.
- [41] A. Florea, D. Busselberg, Cisplatin as an anti-tumor drug: cellular mechanisms of activity, drug resistance and induced side effects, *Cancers* 3 (2011) 1351–1371.
- [42] Y. Gou, J. Li, B. Fan, B. Xu, M. Zhou, F. Yang, Structure and biological properties of mixed-ligand Cu (II) Schiff base complexes as potential anticancer agents, *Eur. J. Med. Chem.* 134 (2017) 207–217.
- [43] Y. Gu, Y. Zhong, M. Hu, H. Li, K. Yang, Q. Dong, H. Liang, Z. Chen, Terpyridine copper(II) complexes as potential anticancer agents by inhibiting cell proliferation, blocking the cell cycle and inducing apoptosis in BEL-7402 cells, *Dalton Trans.* 51 (2022) 1968–1978.
- [44] C. Işcel, V.T. Yılmaz, M. Aygün, M. Erkiş, E. Ulykaya, Novel 5-fluorouracil complexes of Zn(II) with pyridine-based ligands as potential anticancer agents, *Dalton Trans.* 51 (2022) 5208–5217.
- [45] L. Tan, T. Shen, J. Jiang, Y. Zhong, F. Lin, H. Xeu, Y. Yao, X. Jiang, L. Sen, X. He, Bifunctional tetrazole–carboxylate ligand based Zn(II) complexes: synthesis and their excellent potential anticancer properties, *RSC Adv.* 12 (2022) 33808–33815.
- [46] J. tan, B. Wang, L. Zhu, DNA binding, cytotoxicity, apoptotic inducing activity, and molecular modeling study of quercetin zinc (II) complex, *Bioorg. Med. Chem.* 17 (2009) 614–620.
- [47] P. Mondal, A. Bose, Spectroscopic overview of quercetin and its Cu (II) complex interaction with serum albumins, *Bioimpacts* 9 (2019) 115–121.
- [48] Y. Kubota, K. Kubota, S. Tani, DNA binding properties of DAPI (4',6-diamidino-2-phenylindole) analogs having an imidazoline ring or a tetrahydropyrimidine ring: groove-binding and intercalation, *Nucleic Acids Symp. Ser.* 44 (2000) 53–54.
- [49] W.D. Wilson, F.A. Taniou, H.J. Barton, R.L. Jones, K. Fox, R.L. Wydra, L. Strekowski, DNA sequence dependent binding modes of 4', 6-diamidino-2-phenylindole (DAPI), *Biochemistry* 29 (1990) 8452–8461.
- [50] J.Y. Choi, J. Lee, H. Lee, M.J. Jung, S.K. kim, J.M. Kim, DNA-binding geometry dependent energy transfer from 4', 6-diamidino-2-phenylindole to cationic porphyrins, *Biophys. Chem.* 144 (2009) 38–45.
- [51] B. Jana, S. Senapati, D. Ghosh, D. Bose, N. Chattopadhyay, Spectroscopic exploration of mode of binding of ctDNA with 3-hydroxyflavone: a contrast to the mode of binding with flavonoids having additional hydroxyl groups, *J. Phys. Chem. B* 116 (2012) 639–645.
- [52] S. Ghosh, P. Kundu, B.K. Paul, N. Chattopadhyay, Binding of an anionic fluorescent probe with calf thymus DNA and effect of salt on the probe–DNA binding: a spectroscopic and molecular docking investigation, *RSC Adv.* 4 (2014) 63549–63558.
- [53] B.K. Paul, N. Guchhait, Exploring the strength, mode, dynamics, and kinetics of binding interaction of a cationic biological photosensitizer with DNA: implication on dissociation of the drug–DNA complex via detergent sequestration, *J. Phys. Chem. B* 115 (2011) 11938–11949.
- [54] S. Das, G. Suresh Kumar, Molecular aspects on the interaction of phenosafranin to deoxyribonucleic acid: model for intercalative drug–DNA binding, *J. Mol. Struct.* 872 (2008) 56–63.
- [55] S. Ghosh, P. Kundu, N. Chattopadhyay, DNA induced sequestration of a bioactive cationic fluorophore from the lipid environment: a spectroscopic investigation, *J. Photochem. Photobiol. B Biol.* 154 (2016) 118–125.
- [56] J.R. Lakowicz, *Principles of Fluorescence Spectroscopy*, third ed., Plenum, New York, 2006.
- [57] U. Pramanik, L. Khamari, S. Shekhar, S. Mukherjee, On the role of hydrophobic interactions between chloramphenicol and bovine pancreatic trypsin: the effect of a strong electrolyte, *Chem. Phys. Lett.* 742 (2020), 137137.
- [58] P.D. Ross, S. Subramanian, Thermodynamics of protein association reactions: forces contributing to stability, *Biochemistry* 20 (1981) 3096–3102.
- [59] R. Maity, N. Sepay, U. Pramanik, K. Jana, S. Mukherjee, S. Maity, D. Mal, T. Maity, B.C. Samanta, Exploring the noncovalent interactions of the dinuclear Cu (II) Schiff base complex with bovine serum albumin and cell viability against the SiHa cancer cell line, *J. Phys. Chem. B* 125 (2021) 11364–11373.
- [60] J. Zhang, X. Gao, J. Haung, H. Wang, Probing the interaction between human serum albumin and 9-hydroxyphenanthrene: a spectroscopic and molecular docking study, *ACS Omega* (2020) 16833–16840.
- [61] M. Das, P. Brandao, S.S. Mati, S. Roy, A. Anoop, A. James, S. De, U.K. Das, S. Laha, J. Mondal, B.C. Samanta, T. Maity, Effect of ancillary ligand on DNA and protein interaction of the two Zn (II) and Co (III) complexes: experimental and theoretical study, *J. Biomol. Struct. Dyn.* 40 (2021) 14188–14203.
- [62] P. Kundu, N. Chattopadhyay, Interaction of a bioactive pyrazole derivative with calf thymus DNA: deciphering the mode of binding by multi-spectroscopic and molecular docking investigations, *J. Photochem. Photobiol. B* 173 (2017) 485.
- [63] R. Rohs, I. Bloch, H. Sklenar, Z. Shakked, Molecular flexibility in ab initio drug docking to DNA: binding-site and binding-mode transitions in all-atom Monte Carlo simulations, *Nucleic Acids Res.* 33 (2005) 7048–7057.
- [64] D. Seeliger, B.L. de Groot, Ligand docking and binding site analysis with PyMOL and Autodock/Vina, *J. Comput. Aided Mol. Des.* 24 (2010) 417–422.

- [65] O. Trott, A.J. Olson, Auto dock vina: improving the speed and accuracy of docking with a new scoring function, efficient optimization and multithreading, *J. Comput. Chem.* 31 (2010) 455–461.
- [66] S.B. Bukhari, S. Memon, M.M. Tahir, M.I. Bhangar, Synthesis, characterization and antioxidant activity copper–quercetin complex, *Spectrochim. Acta, Part A* 71 (2009) 1901–1906.
- [67] J.E.N. Dolatabadi, A. Mokhtarzadeh, S.M. Gharegraran, G. Dehghan, Synthesis, characterization and antioxidant property of quercetin-Tb(III) complex, *Adv. Pharmaceut. Bull.* 4 (2014) 101–104.
- [68] W. Chen, S. Sun, W. Cao, Y. Liang, J. Song, Antioxidant property of quercetin–Cr(III) complex: the role of Cr(III) ion, *J. Mol. Struct.* 918 (2009) 194–197.
- [69] S.B. Bukhari, S. Memon, M. Mahroof-Tahir, M.I. Bhangar, Synthesis, characterization and antioxidant activity copper–quercetin complex, *Spectrochim. Acta: Mol. Biomol. Spectrosc.* 71 (2009) 1901–1906.
- [70] N. Ghosh, T. Chakraborty, S. Mallick, S. Mana, D. Singha, B. Ghosh, S. Roy, Synthesis, characterization and study of antioxidant activity of quercetin-magnesium complex, *Spectrochim. Acta: Mol. Biomol. Spectrosc.* 151 (2015) 807–813.
- [71] S.B. Bukhari, S. Memon, M.M. Tahir, M.I. Banger, Synthesis, characterization and investigation of antioxidant activity of cobalt–quercetin complex, *J. Mol. Struct.* 892 (2008) 39–46.
- [72] C.J. Adams, T.J. Meade, Gd(III)–Pt(IV) theranostic contrast agents for tandem MR imaging and chemotherapy, *Chem. Sci.* 11 (2020) 2524–2530.
- [73] J. Tan, B. Wang, L. Zhu, DNA binding, cytotoxicity, apoptotic inducing activity, and molecular modeling study of quercetin zinc(II) complex, *bioorg. Med. Chem.* 17 (2009) 614–620.
- [74] J. Tan, B. Wang, L. Zhu, DNA binding and oxidative DNA damage induced by a quercetin copper(II) complex: potential mechanism of its antitumor properties, *J. Biol. Inorg. Chem.* 14 (2009) 727–739.
- [75] V. Barone, M. Cossi, Quantum calculation of molecular energies and energy gradients in solution by a conductor solvent model, *J. Phys. Chem. A* 102 (1998) 1995–2001.
- [76] C. Lee, W. Yang, R.G. Parr, Development of the Colle-Salvetti correlation-energy formula into a functional of the electron density, *Phys. Rev. B* 37 (1998) 785–789.
- [77] M.E. Casida, K.C. Casida, D.R. Salahub, Excited-state potential energy curves from time-dependent density-functional theory: a cross section of Formaldehyde's 1A1 manifold, *Int. J. Quant. Chem.* 70 (1998) 933–948.
- [78] J. Gradinaru, A. Forni, V. Druta, F. Tessore, S. Zecchin, S. Quici, N. Garbalau, Structural, spectral, electric-field-induced second harmonic, and theoretical study of Ni(II), Cu(II), Zn(II), and VO(II) complexes with [N2O2] unsymmetrical schiff bases of S-methylisothiosemicarbazide derivatives, *Inorg. Chem.* 46 (2007) 884–895.
- [79] S. Khan, A.A. Masum, P. Giri, M.M. Islam, K. Harms, S. Chattopadhyay, Chirality-Induced variation in interaction of two similar copper(II) coordination polymers with calf thymus DNA: exploration of their antimicrobial activity and cytotoxicity, *ChemistrySelect* 3 (2018) 7112–7122.
- [80] H.R. Drew, R.M. Wing, T. Takano, C. Broka, S. Tanaka, K. Itakura, R.E. Dickerson, Structure of a B-DNA dodecamer: conformation and dynamics, *Proc. Natl. Acad. Sci. U.S.A.* 78 (1981) 2179–2183.
- [81] F. Yang, C. Bian, L. Zhu, G. Zhao, Z. Huang, M. Huang, Effect of human serum albumin on drug metabolism: structural evidence of esterase activity of human serum albumin, *J. Struct. Biol.* 157 (2007) 348–355.
- [82] J.A. Erickson, M. Jalaie, D.H. Robertson, R.A. Lewis, M. Vieth, Lessons in molecular recognition: the effects of ligand and protein flexibility on molecular docking accuracy, *J. Med. Chem.* 47 (2007) 45–55.
- [83] M. Valko, D. Leibfritz, J. Moncol, M.T. Cronin, M. Mazur, J. Telsler, Free radicals and antioxidants in normal physiological functions and human disease, *Int. J. Biochem. Cell Biol.* 39 (2007) 44–84.
- [84] Y.P. Kwan, T. Saito, D. Ibrahim, F.M.S. Al-Hassan, C.E. Oon, Y. Chen, Jothy, S.L. Jothy, J.R. Kanwar, S. Sasidharan, Polyphenols of frangula alnus and peganum harmala leaves and associated biological activities, *Pharm. Biol.* 54 (2016) 1223–1236.
- [85] P. Subash-babu, D.K. Li, A.A. Alshatwi, In vitro cytotoxic potential of friedelin in human MCF-7 breast cancer cell: regulate early expression of Cdkn2a and pRb1, neutralize mdm2-p53 amalgamation and functional stabilization of p53, *Exp. Toxicol. Pathol.* 69 (2017) 630–636.